Original Article

Institution of MECHANICAL ENGINEERS
Journal of POWER AND ENERGY

Proc IMechE Part A:
J Power and Energy
0(0) 1–14

DOI: 10.1177/0957650917702262
journals.sagepub.com/home/pia
SAGE

Combined effects of viscosity and surface roughness on electric submersible pump performance

MH Siddique[1], Abdus Samad[1] and Afzal Husain[2]

Abstract

An electric submersible pump that lifts crude oil from well bore is a type of multi-stage centrifugal pump. The unexpected wellbore conditions like change in pumping fluid viscosity and sand production severely affect pump performance and eventually lead to breakdown. The present study proposes a numerical approach to understand the effects of fluid viscosity and surface roughness of the flow passages in an electric submersible pump at design and off-design conditions. A three-dimensional numerical analysis was carried out by solving Reynolds-averaged Navier–Stokes equations with shear stress transport turbulence model to characterize performance of the pump. The pumping fluids, i.e., water and crude oils of different viscosities were analyzed for different surface roughness (*Ks*) values. The model predictions were compared with a theoretical one-dimensional model for the effect of viscosity and surface roughness. It was found that the disc-friction and the skin-friction losses are sensitive hydraulic losses of which the disc-friction loss increases with increase in viscosity, whereas skin-friction loss decreases with increase in surface roughness at high viscosity. The combined effect of viscosity and roughness showed a complicated behavior and eventually an improvement in pump performance at a higher surface roughness compared to a smoother and lowers surface roughness.

Keywords

Centrifugal pump, numerical simulation, hydraulic losses, disk friction, skin-friction, crude oil, surface roughness

Date received: 3 January 2017; accepted: 6 March 2017

Introduction

In recent decades, the effect of surface roughness on the performance of centrifugal pump has been studied experimentally as well as numerically by many authors.[1–5] An increase in surface roughness of an electric submersible pump (ESP) impeller hampers its performance and increases the maintenance frequency. The losses caused by the surface roughness are mainly due to the wet friction between the rotating and the stationary part and within the layers of the fluid. Varley[1] studied the effect of surface finish of an impeller experimentally and showed that it decreases the pump efficiency and increases the head because of disc-friction losses. Gulich[2] calculated the effect of roughness on disk friction, fluid rotation and axial thrust. The increase in disc-friction loss for pumping viscous liquid was calculated through power consumption estimation. Li[3] found a sudden head rise and a decrease in hydraulic efficiency of the pump with rough surface or high viscosity fluids. Bai etal.[4] showed that the boundary layer velocity profile becomes plumper and weakens separation bubbles at low Reynolds number (*Re*) when an impeller surface is rough. The increase in surface roughness decreases the efficiency because of the external disc friction.[5] They explained the reason behind the increase in head with the increase in surface roughness.

Viscosity is another major factor which affects the head of a pump. Disk-friction losses and skin-friction losses cause a drop in pump performance.[6] The efficiency of pump with high viscous liquid was obtained by an empirical formula with correction factors.[6] Hydraulic losses because of viscosity depend on roughness pattern, near-wall turbulence and velocity distribution in the passages.[7–10]

[1]Indian Institute of Technology Madras, Chennai, India
[2]Sultan Qaboos University, Muscat, Oman

Corresponding author:
Abdus Samad, Indian Institute of Technology Madras, Chennai, Tamil Nadu 600036, India.
Email: samad@iitm.ac.in

Petroleum industry uses ESPs to lift crude oils and/or water from wellbores. An ESP is a multi-stage centrifugal pump and has stator and rotor mounted in series. A wellbore may contain a multi-phase or multi-component fluid combining two or more phases: liquid (oil or water), gas (natural or dissolved gas) and solid (sand) that make the fluid flow complex and pump performance depreciate to large extents.

To calculate the ESP performance for different fluid viscosities, Sun and Prado[11] modified the equation derived by Sachdeva et al.[12] for incompressible single-phase flow. The modified equations were applicable for different liquid properties and pump speed. El-Naggar[13] explained the losses with one-dimensional flow analysis, but the combined effect of viscosity and surface roughness and the sensitivity of these losses were not studied.

Several researchers[14–18] simulated two-dimensional and three-dimensional equations for flow through centrifugal pumps. Precautions should be taken to select a proper turbulence model for turbulent flows over rough surfaces.[19] Several turbulence models are available such as standard k-ε, RNG k-ε, shear stress transport (SST) and Reynolds stress model, though prediction accuracy depends on its application. An increase in surface roughness increases turbulence near the boundary wall while an increase in Re results in a decrease in boundary layer thickness[5] so, $Y^+ < 5$ need to be maintained to place first mesh point in the viscous sub-layer to avoid error in model predictions.

In the present article, the performance of an ESP is analyzed at various design and off-design conditions to study the combined effect of viscosity and surface roughness. The hydraulic losses and its sensitivity due to surface roughness and viscosity are calculated theoretically as well as numerically. The numerical approach and detailed flow physics have been explained in this article.

Mathematical formulation

Governing equations

The flow analysis in a centrifugal pump can be simplified by assuming three-dimensional incompressible steady-state turbulent flow. The governing equations are Reynolds-averaged Navier–Stokes (RANS) equations with turbulent closure model. Assuming fluid to be incompressible, the mass continuity and momentum equations can be written as

$$\nabla.\vec{v} = 0 \tag{1}$$

and

$$\vec{v}.\nabla\vec{v} = -2\vec{\omega} \times \vec{v} + \omega^2.\vec{r} - \frac{1}{\rho}.\nabla p + \frac{1}{\rho}.\nabla.\vec{\tau} \tag{2}$$

where $\vec{v}$ and ω are the relative fluid velocity and the angular rotation speed of the impeller, respectively, at radial location $\vec{r}$. Fluid pressure is represented by p and the density by ρ; the viscous stress tensor $\vec{\tau}$ includes both the viscous and the turbulence viscosity terms

$$\tau_{ij} = 2\mu.s_{ij} - \overline{\rho.v_i'v_j'} \tag{3}$$

where μ is the fluid viscosity and s_{ij} is the strain tensor. The second term on the right side of the above relation represents the Reynolds stresses due to turbulence motion.

Head equations

A single-phase model for ESP presented by Sun and Prado[11] for head performance derives the head equation without fluid friction and compares it with Euler's head. The total head rise by pump is equal to the impeller head at each stage and is given by

$$H_e = \frac{\omega^2}{g}\left(r_2^2 - r_1^2\right) - \frac{Q}{2\pi g b_1}\left(\frac{1}{\tan\beta_2} - \frac{1}{\tan\beta_1}\right) \tag{4}$$

The total head can be estimated by considering various losses, such as the pump eye head loss, inlet shock circulation head loss, impeller skin-friction head loss and disc-friction head loss. El-Naggar[13] gave simplified one-dimensional equation to estimate these losses. The following losses are hereby calculated by solving equations as shown below.

1. Pump eye head loss (h_{eye})

The head loss at the eye of pump is related to pump head and can be written as

$$h_{eye} = H_m \times C_{eye} \times C_{V_{eye}}^2 \tag{5}$$

where $C_{eye} = 1$ and eye velocity coefficient $C_{V_{eye}}$ is given by

$$C_{V_{eye}} = \frac{V_{eye}}{\sqrt{2 * g * H_m}} \tag{6}$$

where V_{eye} average velocity at the inlet eye of the impeller.

2. Inlet shock circulation head loss (h_{cir})

The inlet shock circulation head loss occurs when the flow discharge is different from the design of impeller inlet tip. The tangential velocity at the inlet of the pump impeller is responsible for this loss which can be estimated as

$$h_{cir} = \frac{W_{u_1} * u_1}{g} \tag{7}$$

where

$$W_{u_1} = u_1\left(1 - \varepsilon\frac{\pi}{Z}\sin\beta_1\right) - V_1\cot(180 - \beta_1) \quad (8)$$

and u_1 is the tangential flow velocity.

3. Impeller skin-friction head loss (h_{sf})

The flow in the impeller passage can be compared to a flow inside a pipe, and to find the impeller skin-friction loss same theory of flow through a pipe can be used.[20] The friction factor can be expressed as

$$h_f = 4C_d\frac{L_b}{D_{hyd}}\frac{W_{av}^2}{2g} \quad (9)$$

where L_b is the length of impeller blade, D_{hyd} is the hydraulic diameter of impeller flow passage, C_d is the impeller dissipation coefficient which can be given as

$$4C_d = (f + 0.006)\left(1.1 + 4\frac{b_2}{D_2}\right) \quad (10)$$

and W_{av} is the average relative velocity which is given by

$$W_{av} = \frac{2Q}{z(d_1b_1 + d_2b_2)} \quad (11)$$

The impeller friction coefficient (f) which is the function of average Reynolds number (Re) and the roughness (Ks) is given by

$$f = \frac{0.3086}{\left\{log\left[\left(\frac{6.9}{Re}\right) + \left(\frac{\frac{Ks}{D_{hyd}}}{3.7}\right)^{1.11}\right]\right\}^2} \quad (12)$$

4. Disk-friction loss (h_{df})

Disk-friction loss is the power loss (P_{ld}) which is due to friction between the fluid and the rotating surface of impeller on both external as well as the internal wall of the impeller. The power loss can be estimated by integrating shear stress (τ) and angular velocity (ω) radically as shown by equation (13). The final expression for (P_{ld}) substituting ($\tau = \frac{f_D}{4}\frac{1}{2}\rho(\omega r)^2$) is given by

$$P_{ld} = \frac{\pi}{40}f_D\rho u_2^3D_2^2 \quad (13)$$

where f_D is the disk-friction coefficient obtained by Kruyt.[21] And the head loss due to disk friction can be estimated by

$$h_{df} = \frac{\pi}{40}\frac{f_D}{g}\frac{u_2^3D_2^3}{Q} \quad (14)$$

Equations (5) to (14) were computed using spread sheet, and losses were calculated through an iterative process. The input parameters are presented in Table 1.

Sand roughness

Surface roughness increases skin-friction loss and can have a significant impact on the performance of the pump. The surface roughness also contributes to the turbulence near the wall which in turns results in the increase of wall shear stress. A technical roughness can have peaks and valleys of different shapes and size (Figure 1), which can be described as equivalent sand-grain roughness.[20]

Proper modeling of a surface is needed for good agreement with the experimental data. In an attempt to describe a curve, Colebrook[22] developed a curve fitting which can be expressed as

$$\frac{1}{\lambda} = 1.74 - 2\log\left(\frac{Ks}{R} + \frac{18.6}{Re_D\sqrt{\lambda}}\right) \quad (15)$$

where Ks is the equivalent Nirkuradse sand-grain roughness value for the surface as shown in

Table 1. Pump specifications.

Parameters	Value
Impeller inlet angle, β_1	30°
Impeller exit angle, β_2	22.5°
Impeller outlet diameter, d_2	100 mm
Number of blades, Z	7
Blade thickness, T	3 mm
Blade length, L_b	0.06 m
Blade width at inlet, b_1	0.0095 m
Blade width at exit, b_2	0.0095 m
Eye diameter, D_1	0.048 m
Blade thickness coefficient, ε_2	0.95
Angular speed, ω	3000
Diffuser inlet angle, β_3	28°
Diffuser exit angle, β_4	81.5°

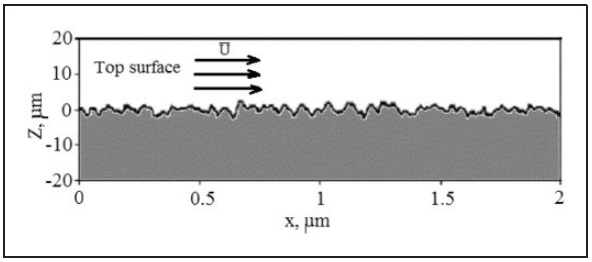

Figure 1. Representative surface roughness.

Figure 2 and λ is the friction factor which can be expressed as

$$\lambda = \frac{-\frac{dp}{dx}}{\frac{1}{2}\rho \bar{U}^2} \tag{16}$$

where $\frac{dp}{dx}$ represents the pressure gradient.

In this study, the mean wall surface roughness value was varied between 0 and 1 mm to find out the effect on the pump performance. And it is assumed that the roughness has blockage effect, which is about 50% of its height to obtain the correct displacement caused by the surface roughness as shown in Figure 2. A non-dimensional roughness factor K which is a ratio of mean roughness value to the hydraulic mean depth of the radial flow (Ks/M) has been used for comparing the results. The hydraulic mean depth of the radial flow at the impeller outlet, M is defined as[1]

$$M = \frac{b_2(2\pi r_2 - ZT\csc\beta_2)}{2(2\pi r_2 - ZT\csc\beta_2 + Zb_2)} \tag{17}$$

Head loss calculation procedure

Equations (5) to (14) were computed using spread sheet, and losses were calculated through an iterative process. The input parameters are presented in Table 1.

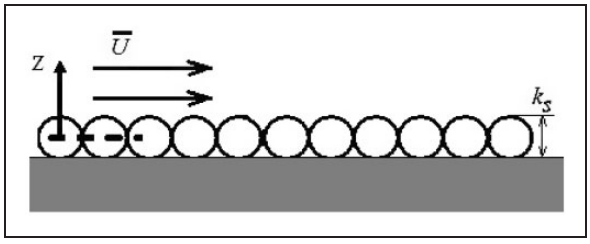

Figure 2. Schematic representation for equivalent sand-grain roughness.

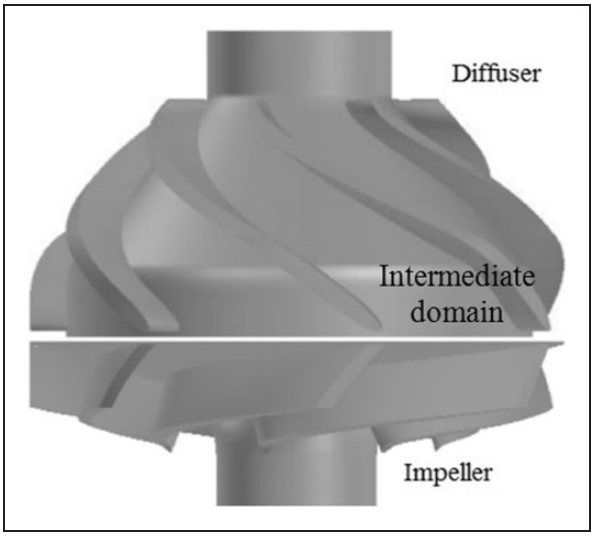

Figure 3. Impeller and diffuser designs.

Computational setup

Geometric modeling

A single-stage ESP[23] was taken for analysis (Figure 3) which consists of three flow domains, i.e., impeller internal flow domain, stationary intermediate domain and the diffuser. The impeller rotates at high angular velocity and thus provides a whirling motion and dynamic head to the fluid. This fluid is

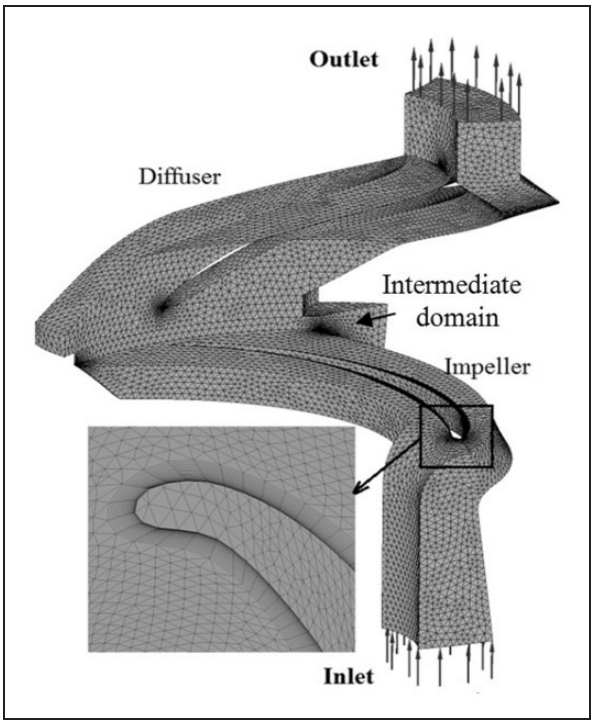

Figure 4. Details of grid system.

Table 2. Mesh statistics and boundary conditions.

Parameter	Description
Flow domain	Impeller, intermediate and diffuser
Interface	Periodic
Mesh	Unstructured
Nodes	504,000
Elements	2,364,000
Fluids	Water and crude oil
Turbulence model	SST
Inlet	Pressure
Outlet	Mass flow rate
Convergence criterion	Residuals $< 1 \times 10^{-5}$
Mass imbalance	0.0124%

SST: shear stress transport.

transmitted to the diffuser through the intermediate domain. The diffuser converts the dynamic head into the pressure head. The geometric details of the computational domain are presented in Table 1. To reduce the computational time, a single impeller passage with periodic boundary condition was taken for analysis (Figure 4). The impeller and the diffuser geometry were prepared separately in ANSYS-*Bladgen* and assembled in ANSYS-*Design Modular*. Further, unstructured mesh was generated through ANSYS-*ICEM*.[24]

Unstructured grid with tetrahedrons, prism and pyramid elements was generated, and an inflation

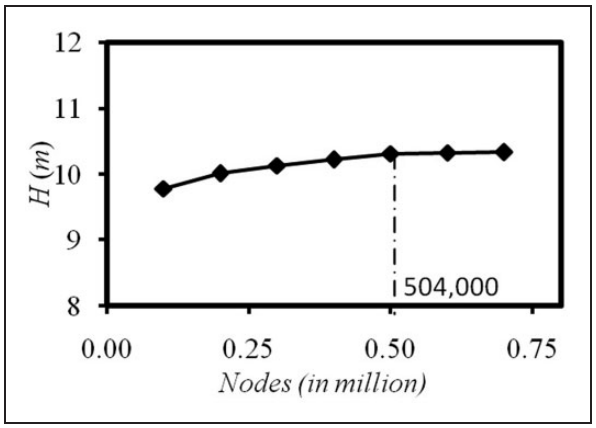

Figure 5. Grid independency.

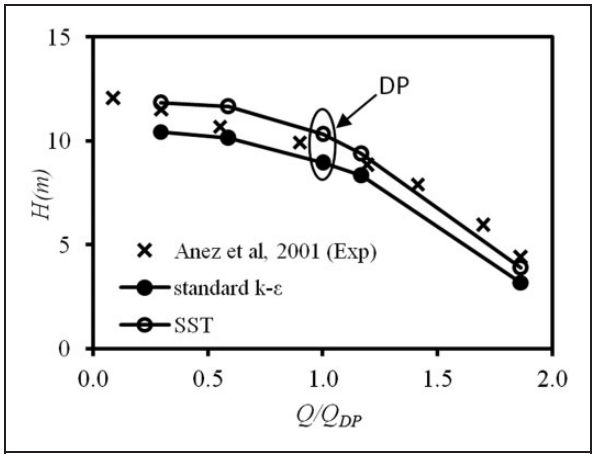

Figure 6. Validation of numerical results using SST and *k-ε* models with experiments of Anez et al.[23]
SST: shear stress transport; DP: design point.

Table 3. Standard deviation of simulated results with SST and k-ε closure model.

Experimental		Numerical			
Q (kg/s)	*H* (m)	SST *H* (m)	*k-ε H* (m)	σ_{SST}	$\sigma_{k-\varepsilon}$
0.96	11.52	11.85	10.45	2.75	4.85
1.78	10.69	11.2	10.15	3.31	3.38
2.92	9.93	10.35	9.25	2.91	3.62
3.88	8.83	9.15	8.10	2.37	3.53
4.58	7.91	7.45	6.50	2.67	4.51
5.51	5.94	5.25	4.45	2.78	3.94
6.05	4.42	3.90	3.19	2.03	3.03

SST: shear stress transport.

Table 4. Fluid properties.

Fluid type	Viscosity (cP)	Density (kg/m^3)
Water	1	1000
C1	40	900
C2	140	939

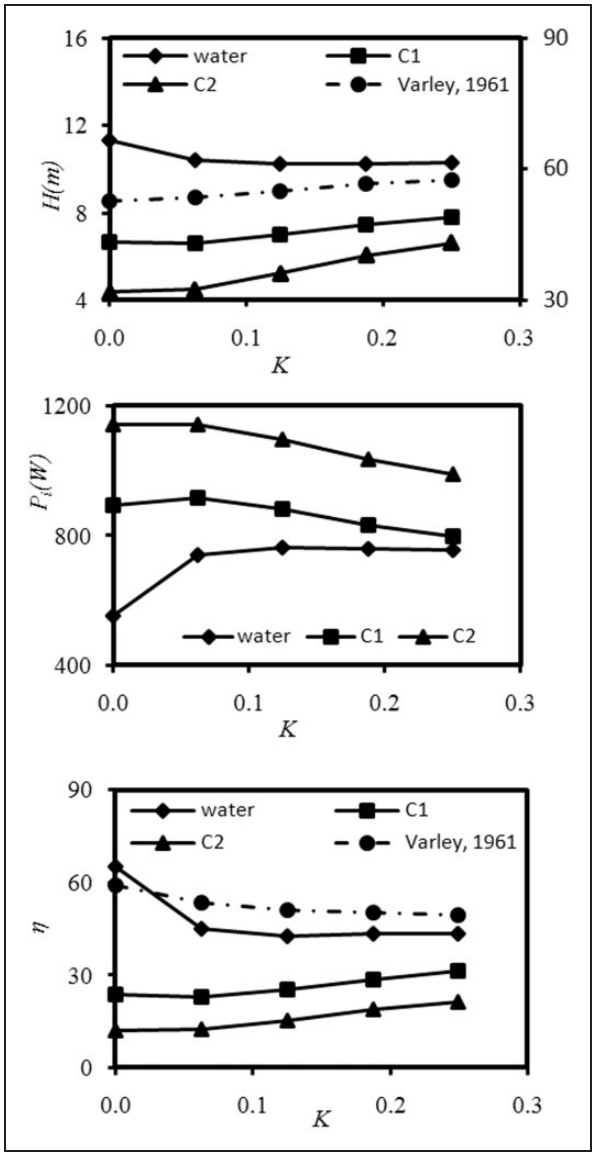

Figure 7. Comparison of head (*H*), input power (P_i) and efficiency (η) at DP for different fluids at increasing roughness obtained numerically.

layer was applied on the impeller blade placing the first layer at a distance of 0.01 mm to capture Y^+ value (=~2) as shown in Figure 4.

Numerical method

The steady-state, RANS equations with turbulence closure model were solved for a single-phase flow. The selection of turbulence model was done through error analysis of standard k-ε and SST. The working fluid was water and crude oil of different viscosities (Table 4). The frozen rotor condition has been used at the interface of stator and rotor. The relative position of the rotor and stator blades was decided by doing simulations at rotational offset from -15° to 60°. The best relative location that is 0° rotational offset gave the closest value to the result when compared with stage average velocity conditions. The mesh statistics and boundary conditions are given in Table 2. The simulations were done at different flow rates. The design point flow rate (Q_{DP}) and speed were 0.003 m^3/s and 3000 r/min, respectively.

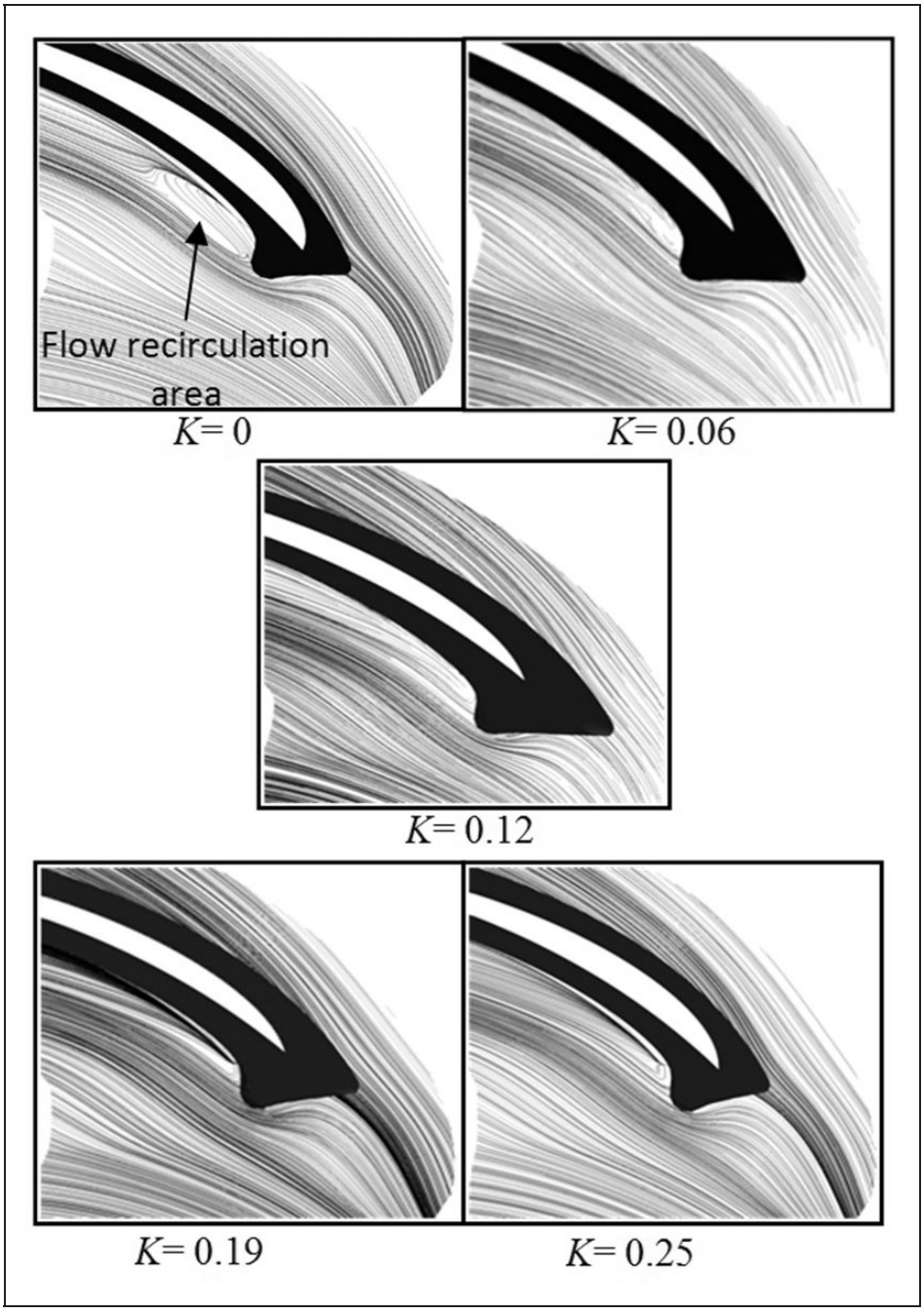

Figure 8. Comparison of streamlines at Q_{DP} for different surface roughness with water as working fluid.

Results and discussion

Grid independency and validation

The grid size plays an important role to get accurate results from the numerical model. The computational time has to be minimized without compromising the accuracy of the results. Grid test was carried out, and the optimal grid was found to be 504,000 nodes after several trials (Figure 5).

The pump performance using standard k-ε and SST models was compared with the experimental results of Anez et al.[23] for water as fluid (Figure 6). The numerical results using SST turbulence model show good agreement with the experimental results. Table 3 shows the percentage error (σ) between the simulated and experimental results at different mass flow rates. The maximum error of simulated results using SST case was found to be 3.31%. The spread of the standard deviation is lower for SST model as compared to k-ε model for the entire range of flow rate. Since SST predicted better results as compared to standard k-ε for all flow rates so, SST was chosen for further analysis.

Effect of roughness

The effect of surface roughness was compared for three different viscosity fluids, water, crude oil (C1) and crude oil (C2), at design and off-design conditions. First of all, theoretical calculations were made by solving equations (5) to (14) to find head losses for all three fluids at different flow rates. Later numerical investigation has been done at different roughness factor $K = 0$, 0.06, 0.12, 0.19 and 0.25 for all the three working fluids to understand qualitatively the effect of surface roughness in the internal flow passages.

The head and efficiency dropped and power increased monotonously with increase of impeller roughness for low viscosity fluid (water). For high viscosity fluids (crude oil C1 and C2), the head and efficiency increased monotonously while power first increased slightly till $K = 0.06$ then decreased further on increase of impeller roughness from $K = 0.06$ to 0.25 (Figure 7).The present result with water as working fluids shows similar trend when compared to experimental results reported by Varley.[1] The result shows that the head and efficiency change non-linearly which matches with the experimental results.

Figure 8 shows surface streamline for water case at 90% span of the impeller inlet for different roughness factor $K = 0$, 0.06, 0.12, 0.19 and 0.25.

A reduction in recirculation at the leading edge of the blade passage can be seen with an increase in surface roughness. The hydraulic losses caused by the recirculation at inlet, generate a lower head up to $K = 0.06$. A further increase in surface roughness from $K = 0.06$ to 0.25 gives increase in the head linearly for water. The minima of the heads disappeared for high viscosity fluids, C1 and C2, and sharp increase in heads was observed from $K = 0.06$ to 0.25. This effect is explained in the next section.

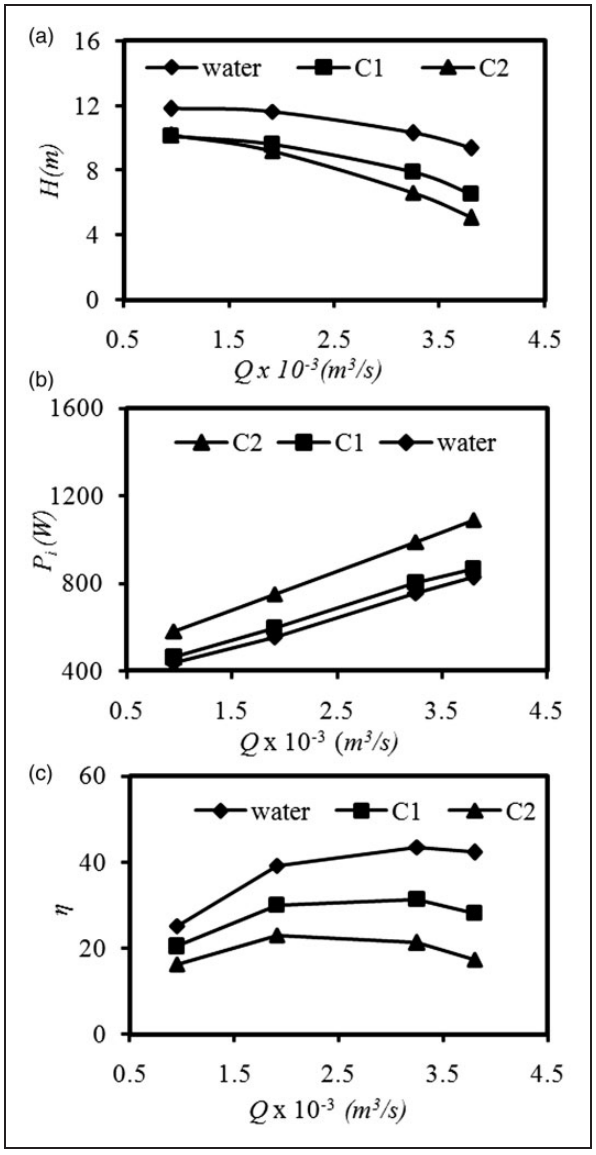

Figure 9. Performance curves of ESP (a) H, (b) η and (c) Pi vs. Q for water, C1 and C2 obtained numerically.

Effect of viscosity

Figure 9(a) to (c) shows total head (H), hydraulic efficiency (η) and input power (P_i) for all three fluid cases with respect to the flow rate calculated numerically. It has been observed from the figure that both head and efficiency drops and input power increases with an increase in viscosity. The change in turbulent to laminar disk-friction losses leads to the drop of pump performance.[25] This effect can be observed by tracing the streamline at design point (Q_{DP}) and at off-design points $0.6Q_{DP}$ and $1.8Q_{DP}$ on the blade surface keeping constant surface roughness factor $K = 0.25$.

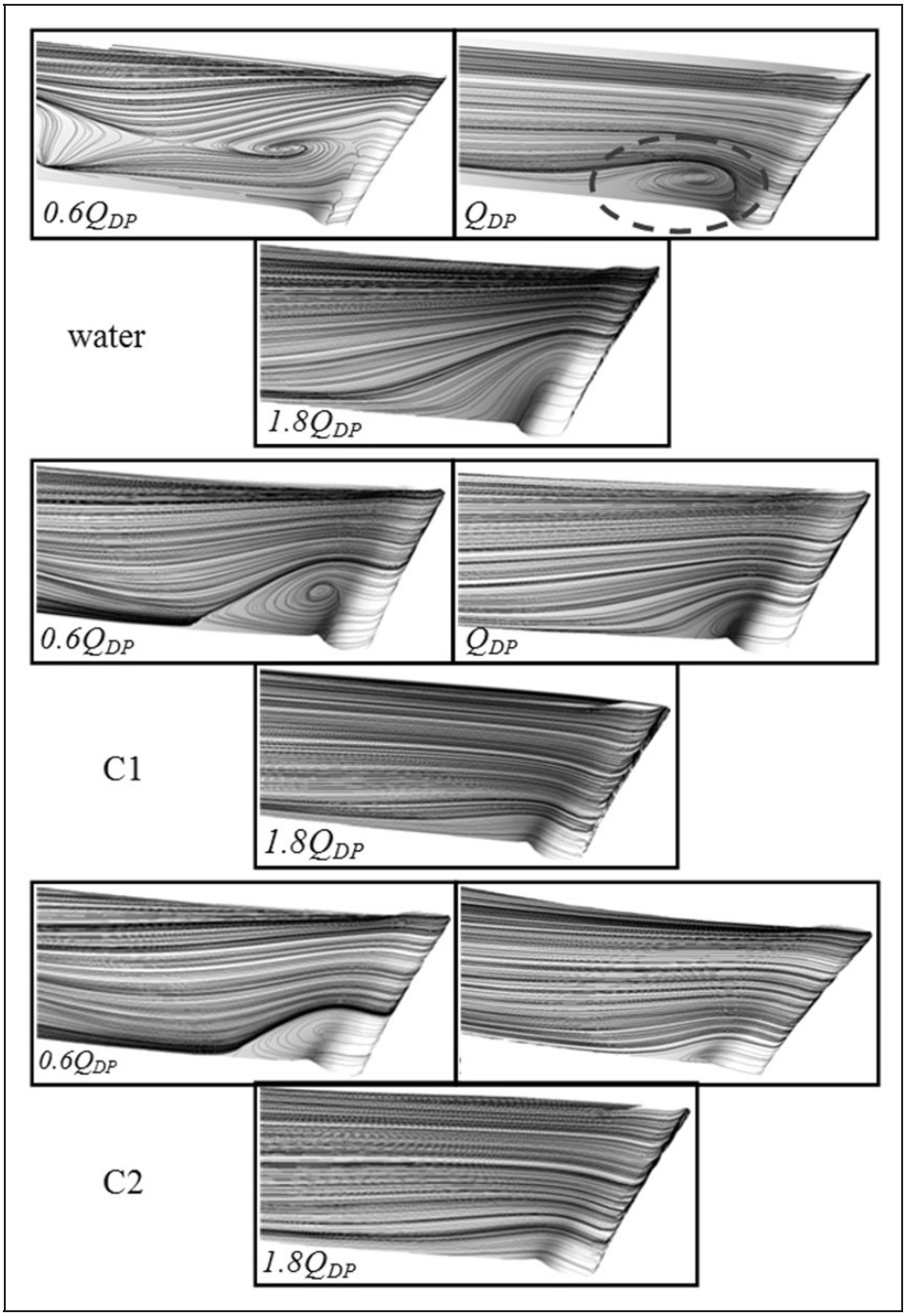

Figure 10. Streamline for impeller blade at $K = 0.25$.

The flow separation and higher turbulent kinetic energy (k) can be seen in case of water at all design points, but in the cases of C1 and C2 the flow separation can be seen only at impeller blade leading edge (LE) of the blade and at 0.6 Q_{DP} (Figures 10 and 11). Figure 11 shows a huge reduction in turbulent kinetic energy (k) at LE and in the flow passages, decreases the turbulent zone and initiates laminar zone. In laminar zone, the average velocity near to wall of blade passage reduces due to increase in skin-friction loss. This increase in skin-friction loss drops the performance of pump for viscous fluids.

Head loss sensitivity

The hydraulic losses such as eye head loss (H_{eye}), inlet shock circulation head loss (H_{cir}), impeller skin-friction head loss (H_{sf}) and disc-friction head loss (H_{df}) were calculated theoretically based on equations (5) to (14) at design and off-design conditions for water, C1 and C2 as working fluids. These losses are then plotted as shown in Figure 12.

The H_{eye} and H_{cir} remain same for all fluids and can be observed a linearly rising with increase of flow rate, but the H_{sf} and H_{df} show different trends

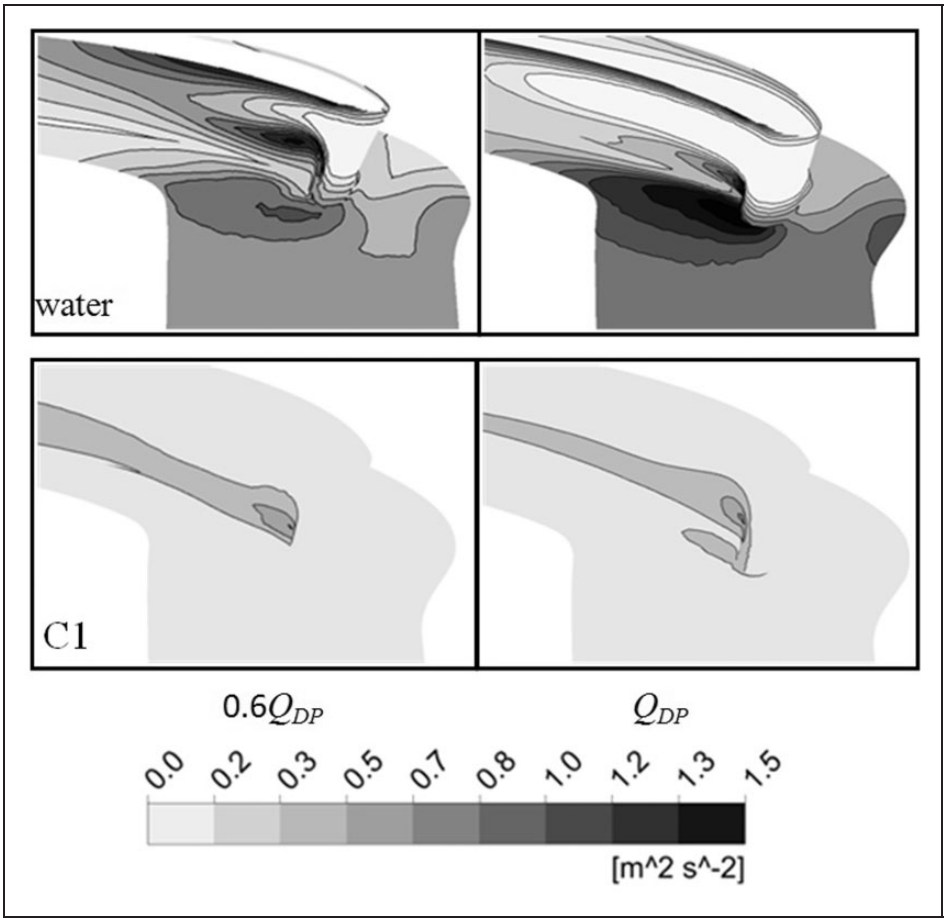

Figure 11. Kinetic energy contours on blade and shroud of the impeller.

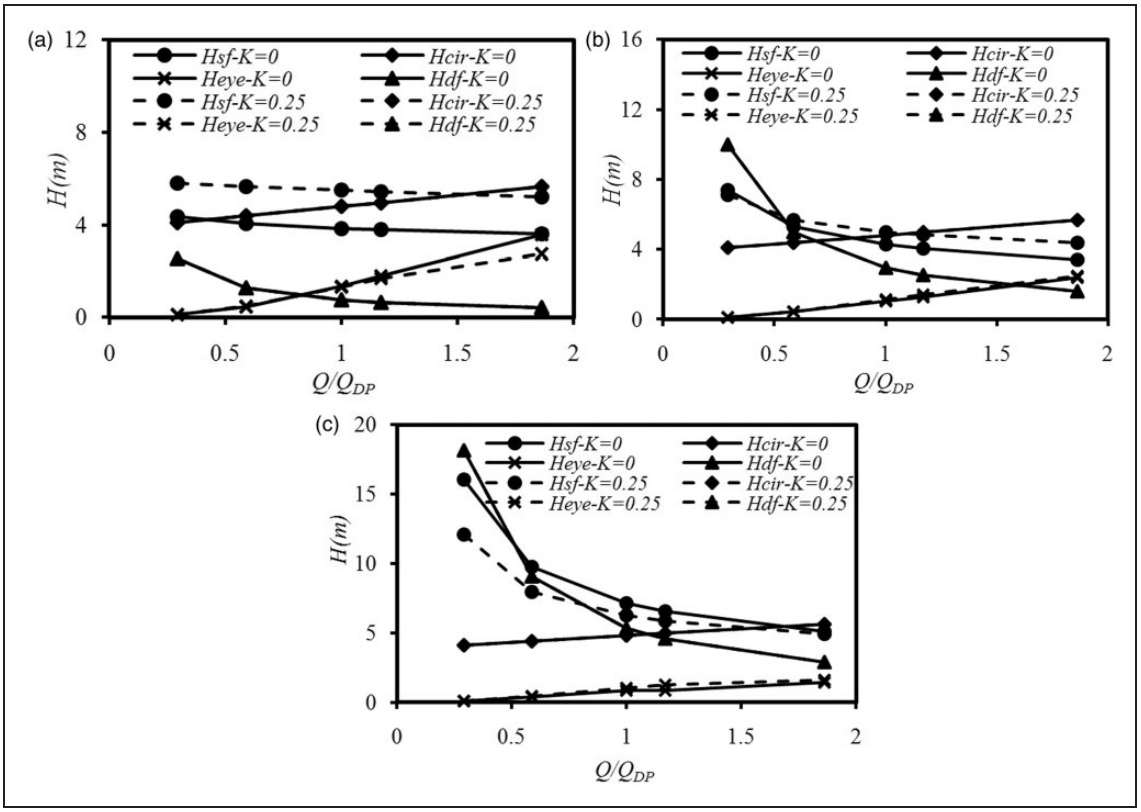

Figure 12. Theoretical head loss sensitivity for different fluids at off-design conditions: (a) water, (b) C1 and (c) C2.

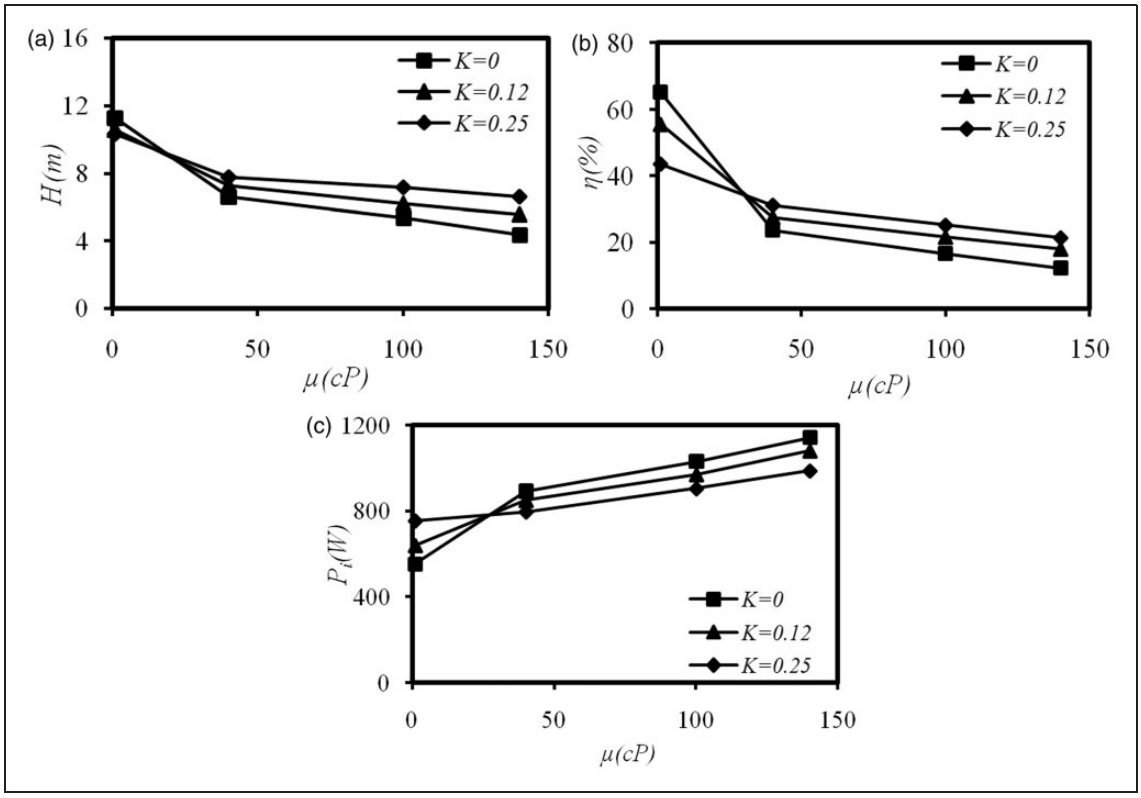

Figure 13. Performance of ESP at different viscosities obtained numerically: (a) head, (b) efficiency and (c) input power.

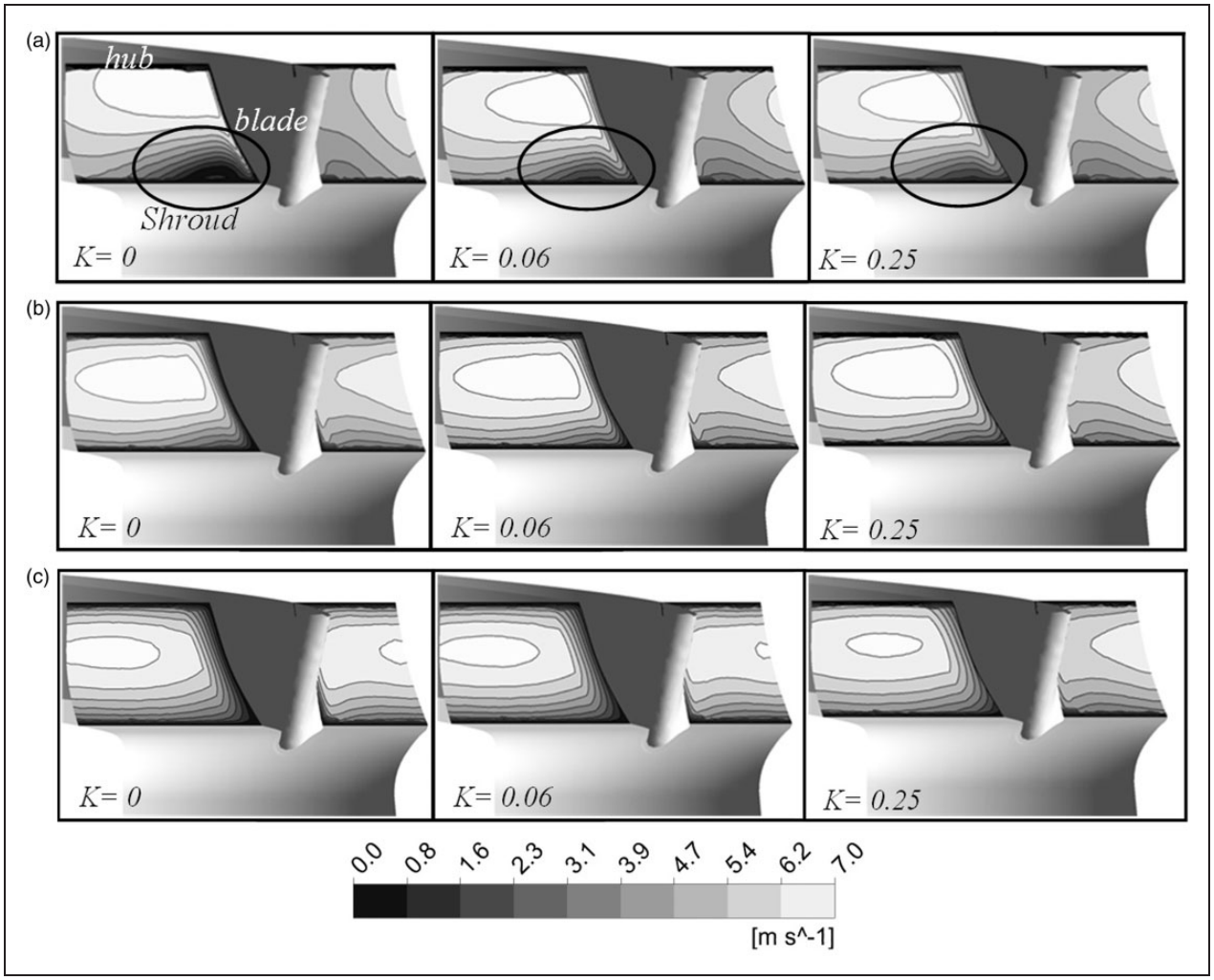

Figure 14. Velocity contours at an arbitrary plane on impeller: (a) water, (b) C1 and (c) C2.

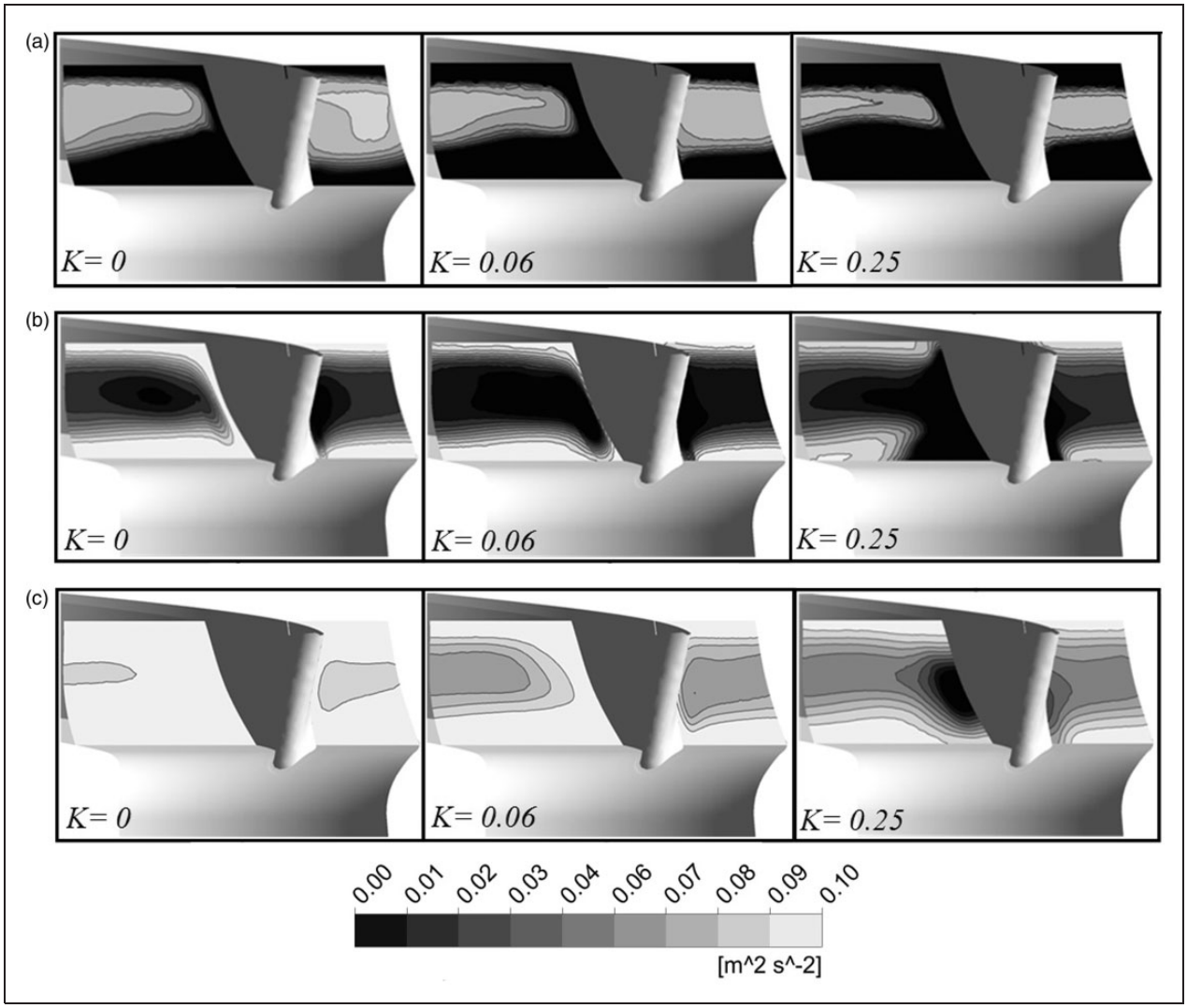

Figure 15. Kinetic energy contours at an arbitrary plane on impeller: (a) water, (b) C1 and (c) C2.

at smooth and rough surface ($K = 0.25$) for water and C1, C2.

Figure 12 also shows that the H_{df} is higher for viscous fluids as compared to the H_{sf}. At off-design conditions, i.e., at a low discharge, both H_{sf} and H_{df} are high for high viscous fluids (C1 and C2). The H_{sf} for $K = 0$ is lesser than for $K = 0.25$ in case of water (Figure 12(a)). But, as the viscosity increases in Figure 12(b) and (c), the H_{sf} for $K = 0$ increases as compared to $K = 0.25$, and in Figure 12(c) the H_{sf} for $K = 0$ becomes more than that at $K = 0.25$. This shows that the H_{sf} is more sensitive toward viscosity than that of other hydraulic losses.

Combined effect of surface roughness and viscosity

Simulations were carried out for $K = 0$ to 0.25 for water, C1 and C2. The Euler head and the hydraulic head losses are defined by equations (4) and (5) to (14), respectively. The overall pump performance deteriorates by considering the combined effect of viscosity and surface roughness (Figure 13). This is because the effect of viscosity on the performance of the pump is more dominating then the effect of surface roughness (Figure 7).

A decrease in pump performance caused by friction and flow separation[20,26] leads to hydraulic head losses as discussed above. The viscosity of fluid and the local coefficient of friction (C_f) is closely associated to the disk-friction loss. An increase in friction forces on the surface of a rotating part and the shear stress to the local coefficient of friction (C_f) are given by

$$\tau = \frac{1}{2}\rho \times c_f \times u^2 \tag{18}$$

where $u = \omega \times r$. The friction forces on the surface can be given as

$$dF = 2\pi \times \tau \times r \times dr \tag{19}$$

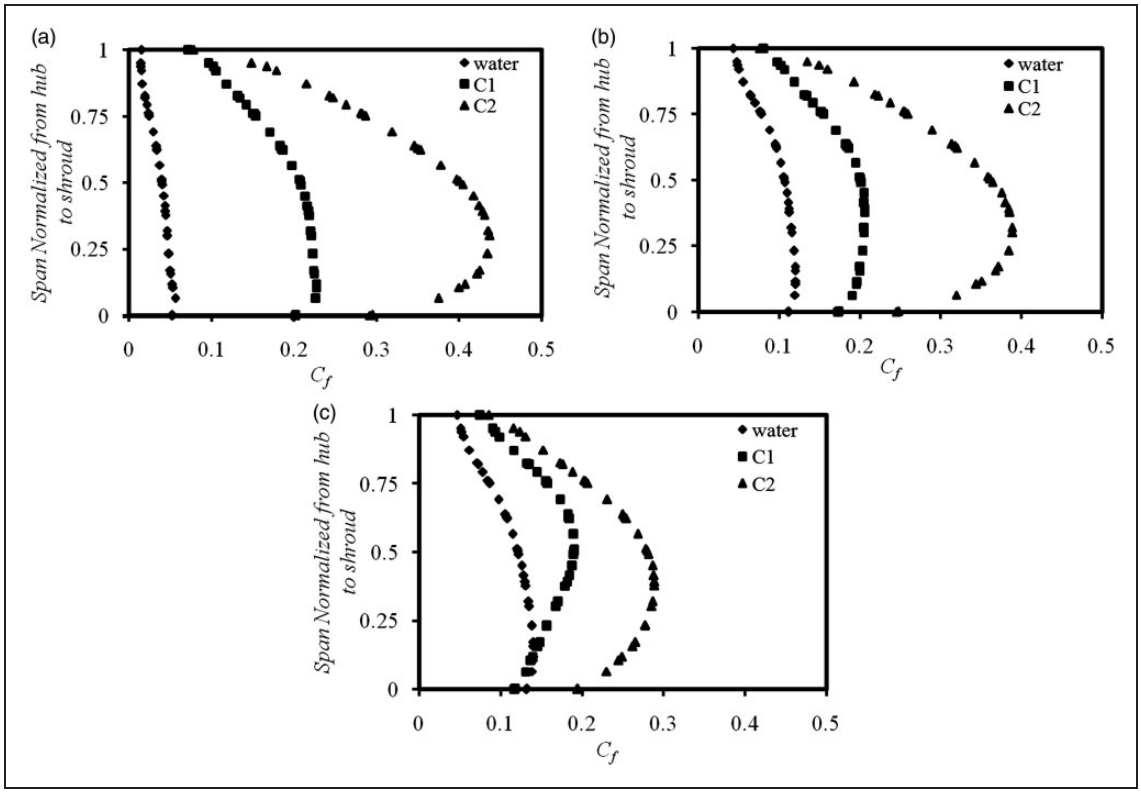

Figure 16. Coefficient of friction at a polyline near to blade of the impeller obtained numerically: (a) $K = 0$, (b) $K = 0.06$ and (c) $K = 0.25$.

The velocity and turbulent kinetic energy contours are shown in Figures 14 and 15, respectively. The velocity and turbulent kinetic energy distribution change significantly with the change in surface roughness and fluid viscosity.

An increase in surface roughness increases the flow resistance due to turbulence near to the wall of a flow passage. This happens only when roughness protrudes beyond the laminar sub-layers.[27,28] The above phenomenon can be identified from Figure 15. In this the region of high turbulent kinetic energy (k) for both $K = 0$ and $K = 0.06$ is almost same for all fluids. But, when K increases to 0.25, the high k region shifts toward the blade surface can be easily seen in C1 and C2 (Figure 15). This gave small rise in streamline velocity near to the blade region of the impeller which can be easily seen in water case (Figure 14).

Now, shear stress is the function of the coefficient of friction (C_f) and the velocity as shown in equation (18). Plotting C_f across the normalized span closer to the impeller blade wall shown in Figure 16 shows decrease in C_f for viscous fluids C1 and C2 with the increase of surface roughness. Due to the decrease in local coefficient of friction (C_f) and a small rise in velocity, decreases the shear stress over the blade and gives a rise in head and efficiency for high viscous fluid compared to less viscous fluids (Figure 13).

Conclusion

The effects of roughness and viscosity of fluid on the ESP performance were studied through a three-dimensional numerical and one-dimensional theoretical analysis. The conclusions are:

- The performance decreases with the increase in viscosity, but the head increases with the increase in surface roughness factor (K) for $K > 0.06$.
- The effects of K are more prominent for high viscosity fluids.
- An increase in turbulent kinetic energy due to surface roughness near to the surface of blade improves the head. This effect is more for high viscosity fluids.
- The increase in turbulent kinetic energy (k) decreases the frictional force between the viscous layers and helps in increasing the absolute fluid velocity and the total head.
- The disc-friction and the skin-friction losses are sensitive hydraulics losses of which the disc-friction loss increases with the increase in viscosity whereas, skin-friction loss decreases with the increase of surface roughness at high viscosity.

If proper surface roughness is maintained at each stage of an ESP, then the losses can be minimized for pumping viscous fluids and this will significantly reduce the pumping cost.

Declaration of Conflicting Interests

The author(s) declared no potential conflicts of interest with respect to the research, authorship, and/or publication of this article.

Funding

The author(s) received no financial support for the research, authorship, and/or publication of this article.

References

1. Varley FA. Effects of impeller design and surface roughness on the performance of centrifugal pumps. *Proc Inst Mech Eng* 1961; 175: 955–969.
2. Gülich JF. Disk friction losses of closed turbomachine impellers. *Forsch im Ingenieurwesen/Eng Res* 2003; 68: 87–95.
3. Li WG. Effect of exit blade angle, viscosity and roughness in centrifugal pumps investigated by CFD computation. *Task Q* 2011; 15: 21–41.
4. Bai T, Lui J, Zhang W, et al. Effect of surface roughness on the aerodynamic performance of turbine blade cascade. *Propuls Power Res* 2011; 3: 82–89.
5. Bellary SAI and Samad A. Pumping crude oil by centrifugal impeller having different blade angles and surface roughness. *J Pet Explor Prod Technol* 2015; 6: 117–127.
6. Stepanoff AJ. Pumping viscous oils with centrifugal pump. *Oil Gas J* 1940; 1: 26–28.
7. Li WG. Effects of viscosity of fluids on centrifugal pump performance and flow pattern in the impeller. *Int J Heat Fluid Flow* 2000; 21: 207–212.
8. Gülich JF. Effect of Reynolds number and surface roughness on the efficiency of centrifugal pumps. *J Fluids Eng* 2003; 125: 670–679.
9. Li WG. Numerical study on behavior of a centrifugal pump when delivering viscous oils – Part 1: Performance. *Int J Turbo Jet Engines* 2008; 25: 61–79.
10. Denney D. Influence of viscosity on ESP performance. *J Pet Technol* 2008; 60: 57–59.
11. Sun D and Prado M. Single-phase model for ESP's head performance. In: *SPE production and operations symposium*, Oklahoma City, USA, 2003.
12. Sachdeva R, Doty D and Schmidt Z. Performance of electric submersible pumps in gassy wells. In: *66th annual technical conference and exhidition of SPE*, Dallas,USA, 6–9 October 1991.
13. El-Naggar M. A one-dimensional flow analysis for the prediction of centrifugal pump performance characteristics. *Int J Rotatiing Mach* 2013; 2013: 1–19.
14. Dawes WN. A numerical method for the analysis of 3D viscous compressible flow in turbine cascades; Application to secondary flow development in a cascade with and without dihedral. In*: International Gas Turbine Conference and Exhibition*, Dusseldorf, Germany, 8-12 June 1986.
15. Goto A. Study of internal flows in a mixed-flow pump impeller at various tip clearances using 3D viscous flow computations. *Am Soc Mech Eng* 1992; 114: 373–382.
16. Croba D and Kueny JL. Numerical calculation of 2D, unsteady flow in centrifugal pumps: impeller and volute interaction. *Int J Numer Method Fluids* 1996; 22: 467–481.
17. Stickland MT and Scanlon TJ. Numerical flow simulation in a centrifugal pump with impeller-volute interaction. In: *Proceeding of ASME FEDSM'00, fluid engineering division summer meeting*, Boston, USA, 2000, pp.1–7. http://strathprints.strath.ac.uk/7436/%0AStrathprints (accessed 20 March 2017).
18. ShojaeeFard MH, Boyaghchi FA and Ehghaghi MB. Experimental study and three-dimensional numerical flow simulation in a centrifugal pump when handling viscous fluids. *IUST Int J Eng Sci* 2006; 17: 53–60.
19. Robertson JM, Martin JD and Brukhart TH. Tubulent flow in rough pipes. *Ind Eng Chem Fundam* 1968; 7: 253–265.
20. Nikuradse J. *Laws of flow in rough pipes*. NACA Technical memorandum 1292, July–August 1933. DOI: 10.1063/1.1715007.
21. Kruyt NP. *Lecture notes: fluid mechanics of turbomachines II*. In: Turbomachinery Laboratory. Amsterdam, The Netherlands: University of Twente, 2009.
22. Colebrook CF. Turbulent flow in pipes, with particular references to the transition region between the smooth and rough pipe laws. *J Inst Civ Eng* 1939; 11: 133–156.
23. Anez D, Kenyery F and Escalante S. Teran VM. ESP's performance with two-phase and viscous flow. In: *Proceeding of ETCE, petroleum production technology symposium*, Houston, USA, 2001.
24. ANSYS ICEM CFD User's manual, ANSYS 15, ANYSY Inc. (2013).
25. Ippen A. The influence of viscosity on centrifugal performance. *Trans ASME* 2012; 68: 1–18.
26. Gulich J. *Centrifugal pump*. 2nd ed. Berlin: Springer Publications, 2010.
27. Schlichting H. *Boundary layer theory*. 7th ed. New York: MaGraw-Hill, 1979.
28. Trinh KT. *On the critical Reynolds number for transition from laminar to turbulent flow* 2010; 39. https://arxiv.org/ftp/arxiv/papers/1007/1007.0810.pdf (accessed 20 March 2017).

Appendix

Notation

Symbols

b	blade width
C	coefficient
C1, C2	crude oils
d	impeller outlet diameter, mm
D	eye diameter, mm
g	acceleration due to gravity, m/s^2
H	total head, m
k	turbulence kinetic energy, m^2/s^2
K	non-dimensional roughness factors
Ks	mean grain size, mm
L	chord length, mm
M	hydraulic mean depth of impeller outlet
P	pressure, N/m^2
Pi	input power, W
Q	volume flow rate, m^3/s
r	radius, mm
Re	Reynolds number
t	time, s
T	blade thickness, mm

Z	number of blades
β	blade angle, $^\circ$
ε	rate of kinetic energy dissipation, J/s
η	hydraulic efficiency
μ	viscosity, cP
ρ	density, kg/m^3
σ	percentage error
ω	angular speed, r/min

Subscripts

cal	theoretical calculation
cfd	computational fluid dynamics
cir	loss due to inlet shock circulation
df	loss due to disc friction
DP	design point
e	Euler
eye	loss at eye of pump
f	friction
m	manometric
sf	loss due to skin friction
1	inlet impeller
2	exit impeller
3	inlet diffuser
4	exit diffuser